9. K. A. Guss, C. E. Nelson, A. Hudson, M. E. Kraus, S. B. Carroll, *Science* **292**, 1164–1167 (2001).
10. G. H. Wei *et al.*, *EMBO J.* **29**, 2147–2160 (2010).
11. G. Badis *et al.*, *Science* **324**, 1720–1723 (2009).
12. A. Jolma *et al.*, *Cell* **152**, 327–339 (2013).
13. K. R. Nitta *et al.*, *eLife* **4**, e04837 (2015).
14. M. A. Hume, L. A. Barrera, S. S. Gisselbrecht, M. L. Bulyk, *Nucleic Acids Res.* **43**, D117–D122 (2015).
15. H. Zhang, M. Levine, H. L. Ashe, *Genes Dev.* **15**, 261–266 (2001).
16. J. Crocker *et al.*, *Cell* **160**, 191–203 (2015).
17. S. Small, R. Kraut, T. Hoey, R. Warrior, M. Levine, *Genes Dev.* **5**, 827–839 (1991).
18. C. I. Swanson, D. B. Schwimmer, S. Barolo, *Curr. Biol.* **21**, 1186–1196 (2011).
19. J. Jiang, M. Levine, *Cell* **72**, 741–752 (1993).
20. R. W. Lusk, M. B. Eisen, *PLOS Genet.* **6**, e1000829 (2010).
21. M. M. Kulkarni, D. N. Arnosti, *Mol. Cell. Biol.* **25**, 3411–3420 (2005).
22. C. I. Swanson, N. C. Evans, S. Barolo, *Dev. Cell* **18**, 359–370 (2010).
23. A. Muhlethaler-Mottet *et al.*, *J. Biol. Chem.* **279**, 40529–40535 (2004).
24. D. Panne, T. Maniatis, S. C. Harrison, *Cell* **129**, 1111–1123 (2007).
25. W. Shi, M. Levine, *Development* **135**, 931–940 (2008).
26. H. Yasuo, C. Hudson, *Dev. Biol.* **302**, 92–103 (2007).
27. A. Stolfi, E. Wagner, J. M. Taliaferro, S. Chou, M. Levine, *Development* **138**, 5429–5439 (2011).
28. E. Wagner, M. Levine, *Development* **139**, 2351–2359 (2012).
29. W. A. Whyte *et al.*, *Cell* **153**, 307–319 (2013).
30. D. Hnisz *et al.*, *Cell* **155**, 934–947 (2013).
31. Q. Li, K. R. Peterson, X. Fang, G. Stamatoyannopoulos, *Blood* **100**, 3077–3086 (2002).
32. G. M. Clore, A. Bax, J. G. Omichinski, A. M. Gronenborn, *Structure* **2**, 89–94 (1994).
33. R. Kodandapani *et al.*, *Nature* **380**, 456–460 (1996).

ACKNOWLEDGMENTS

Sequencing data for this project have been deposited in the National Center for Biotechnology Information, NIH, Sequencing Read Archive (www.ncbi.nlm.nih.gov/sra), PRJNA294804. We thank M. Chung, C. Anderson, E. Wagner, J. Lyons, and members of the Levine and Rokhsar labs for helpful discussions. This work was supported by grants from the NIH (GM46638 and NS076542). There are no conflicts of interest to declare. Author contributions are as follows: E.K.F., D.S.R., and M.S.L. devised experiments; E.K.F. and K.M.O. performed experiments; W.Z. designed and executed bioinformatics analysis; A.J.B. conducted bioinformatics analyses; and E.K.F., D.S.R., and M.S.L. wrote the paper. All authors discussed the results and commented on the manuscript. M.S.L., D.S.R., and E.K.F. have filed a patent application (no. 62/169,458) that relates to the production of enhancer variants using the SEL-Seq method.

SUPPLEMENTARY MATERIALS

www.sciencemag.org/content/350/6258/325/suppl/DC1
Materials and Methods
Figs. S1 to S14
Tables S1 to S4
References (*34*–*41*)

29 May 2015; accepted 10 September 2015
10.1126/science.aac6948

T CELL IMMUNITY

RIPK1 and NF-κB signaling in dying cells determines cross-priming of CD8$^+$ T cells

Nader Yatim,[1,2,3] Hélène Jusforgues-Saklani,[1,2] Susana Orozco,[4] Oliver Schulz,[5] Rosa Barreira da Silva,[1,2] Caetano Reis e Sousa,[5] Douglas R. Green,[6] Andrew Oberst,[4] Matthew L. Albert[1,2]*

Dying cells initiate adaptive immunity by providing both antigens and inflammatory stimuli for dendritic cells, which in turn activate CD8$^+$ T cells through a process called antigen cross-priming. To define how different forms of programmed cell death influence immunity, we established models of necroptosis and apoptosis, in which dying cells are generated by receptor-interacting protein kinase-3 and caspase-8 dimerization, respectively. We found that the release of inflammatory mediators, such as damage-associated molecular patterns, by dying cells was not sufficient for CD8$^+$ T cell cross-priming. Instead, robust cross-priming required receptor-interacting protein kinase-1 (RIPK1) signaling and nuclear factor κB (NF-κB)–induced transcription within dying cells. Decoupling NF-κB signaling from necroptosis or inflammatory apoptosis reduced priming efficiency and tumor immunity. Our results reveal that coordinated inflammatory and cell death signaling pathways within dying cells orchestrate adaptive immunity.

Phagocytosis of dying cells by dendritic cells (DCs) results in cross-presentation of cell-associated antigen and the priming of CD8$^+$ T cells (*1*). This pathway mediates the processing and presentation of tumor antigens (*2*), as well as viral and self proteins in instances where expression is restricted to nonhematopoietic cells (*3*, *4*). However, the manner by which different forms of programmed cell death (PCD) influence the ability of DCs to cross-present and initiate CD8$^+$ T cell responses is still poorly understood.

Until recently, apoptosis was thought to be immunologically quiescent, in contrast to necrosis, which is characterized by rapid membrane permeabilization and the release of inflammatory mediators called damage-associated molecular patterns (DAMPs). Paradoxically, the inflammatory nature of necrotic cells (defined by their ability to activate innate immune cells) (*5*–*8*) does not correlate with their ability to serve as a source of antigen for the initiation of CD8$^+$ T cell immunity (defined as immunogenicity) (*1*, *9*–*12*). Moreover, immunogenic cell death has often been associated with apoptotic pathways (*1*, *10*, *13*–*15*). Several recent studies highlighted the interconnections between cell death and inflammatory signal transduction. For example, proteins such as receptor-interacting protein kinase-3 (RIPK3) and caspase-8, which respectively initiate necroptosis and apoptosis, are incorporated into dynamic innate immune signaling modules (e.g., ripoptosome) (*16*–*19*). These cytosolic scaffolds establish the cross-talk between innate immune and cell death programs, and, in some instances, both pathways may be simultaneously engaged (fig. S1A). This integration of pathways, combined with the recent discovery of necroptosis (a regulated form of necrosis), prompted us to reevaluate how different PCD pathways affect cross-priming of CD8$^+$ T cells.

To selectively induce apoptosis or necroptosis, we constructed "pure" cell death systems, in which the death effector proteins caspase-8 or RIPK3 were fused to a modified FK506 binding protein (FKBP) domain (Fv-ΔN-caspase-8 and RIPK3-2xFv, respectively) (*20*–*22*) (fig. S1B). RIPK3 oligomerization results in the recruitment of RIPK1 via interactions with the RIPK3–RIP homotypic interaction motif (RHIM^{RIPK3}) domain, leading to the formation of a cytosolic ripoptosome-like complex (*21*, *23*). Therefore, we also generated a C-terminally truncated construct (RIPK3ΔC-2xFv) (fig. S1B), which lacks the RHIM^{RIPK3} domain and does not recruit RIPK1 (*21*). NIH 3T3 cells were stably transduced with these activatable constructs (referred to herein as acC8, acR3, and acR3ΔC). Dimerization of caspase-8 resulted in the induction of apoptosis, whereas oligomerization of full-length RIPK3 and RHIM-less RIPK3 induced rapid cell swelling and membrane rupture (<3 hours) in the absence of caspase activation (Fig. 1, A and B; fig. S2, A to C; and movies S1 to S3). The ability to induce necroptosis in the absence of the RHIM^{RIPK3} domain enabled us to decouple the formation of RIPK1-dependent ripoptosome complex from cell death (*21*), hence eliminating the activation of other pathways emanating from the ripoptosome.

Cell death–associated molecules such as calreticulin (CRT), adenosine triphosphate (ATP), and high-mobility group box-1 (HMGB1) have been shown to trigger inflammation and to regulate immunogenic cell death (*8*, *15*, *24*–*26*). We therefore quantified CRT surface exposure and the

[1]Laboratory of Dendritic Cell Biology, Department of Immunology, Institut Pasteur, 25 Rue du Docteur Roux, 75015 Paris, France. [2]Institut National de la Santé et de la Recherche Médicale, U818, 25 Rue du Docteur Roux, 75015 Paris, France. [3]Frontières du Vivant Doctoral School, École Doctorale 474, Université Paris Diderot-Paris 7, Sorbonne Paris Cité, 8-10 Rue Charles V, 75004 Paris, France. [4]Department of Immunology, University of Washington, Campus Box 358059, 750 Republican Street, Seattle, WA 98109, USA. [5]Immunobiology Laboratory, The Francis Crick Institute, Lincoln's Inn Fields Laboratory, 44 Lincoln's Inn Fields, London WC2A 3LY, UK. [6]Department of Immunology, St. Jude Children's Research Hospital, 262 Danny Thomas Place, Memphis, TN 38105, USA.
***Corresponding author. E-mail: albertm@pasteur.fr**

Downloaded from http://science.sciencemag.org/ on August 30, 2016

release of both ATP and HMGB1 by apoptotic or necroptotic cells. Low levels of CRT exposure were observed during the three forms of cell death, and only the acR3- and acR3ΔC-expressing NIH 3T3 cells rapidly released high concentrations of ATP and HMGB1 upon treatment (Fig. 1, C to E). In all cases, no detectable levels of interleukin-1α (IL-1α), IL-1β, or uric acid were released. We next evaluated phagocytosis by DCs (i.e., acquisition of antigen) and subsequent DC maturation, which are two steps required for achieving $CD8^+$ T cell cross-priming (*27*, *28*). We found that bone marrow–derived dendritic cells (BMDCs) and a $CD8\alpha^+$ DC–derived cell line (MuTuDC) acquired similar amounts of dimerizer-treated acC8-, acR3-,

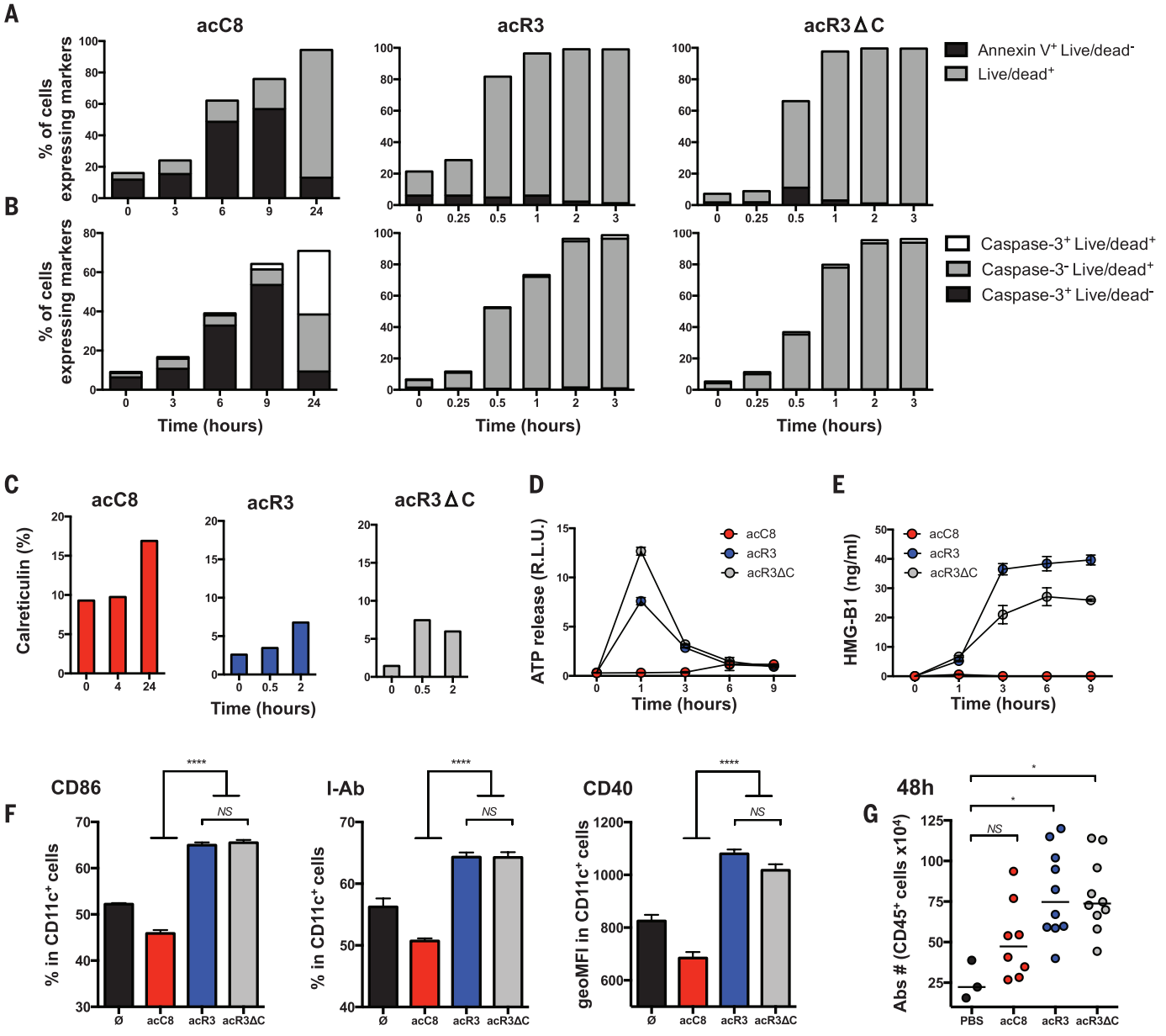

Fig. 1. Necroptotic cells release DAMPs and induce dendritic cell maturation. (**A** to **C**) NIH 3T3 cells expressing the death constructs were stimulated with dimerizer. Cells were harvested at the indicated times and stained with Annexin-V and Live/Dead reagent (A); cleaved caspase-3 antibody and Live/Dead reagent (B); or CRT antibody (C). Cells that are Annexin V^+ Live/$Dead^-$ (indicating phosphatidylserine exposure before membrane permeabilization) or cleaved caspase-3^+ (indicating the activation of executioner caspases) are undergoing apoptosis. At later times (24 hours), staining with Live/Dead reagent indicates a loss of plasma membrane integrity and characterizes secondary necrotic cells. Rapid membrane permeabilization without activation of executioner caspases (caspase-3^- Live/$Dead^+$) is a feature of necroptosis. Results are from one representative experiment ($n = 2$ independent experiments). (**D** and **E**) ATP and HMGB1 were quantified from dying cell culture supernatants. Results are reported as means (± SEM) of triplicates of one representative experiment ($n = 3$ independent experiments). (**F**) BMDCs were cocultured with dimerizer-treated acC8-, acR3-, and acR3ΔC-expressing cells for 24 hours. DC maturation phenotypes were assessed by flow cytometry. Results are reported as in (D) and (E) ($n = 4$ independent experiments). (**G**) 2×10^6 dimerizer-treated cells were injected into the peritoneal cavity of WT C57BL/6 mice. Forty-eight hours later, peritoneal cells were collected, and immune cells were enumerated by cytometry. Bars indicate means of two pooled independent experiments with four to five mice per group [except in the phosphate-buffered saline (PBS) group]. Each circle represents one mouse. *P* values for (F) were determined by the one-way ANOVA test; *P* values for (G) were determined by the Kruskal-Wallis test (multigroup comparision), followed by Dunn's post-test, comparing each group to the PBS group. $*P < 0.05$; $****P < 0.0001$; NS, not significant. acC8, caspase-8 apoptosis; acR3, RIPK3 necroptosis; acR3ΔC, RHIM-less RIPK3 necroptosis.

Downloaded from http://science.sciencemag.org/ on August 30, 2016

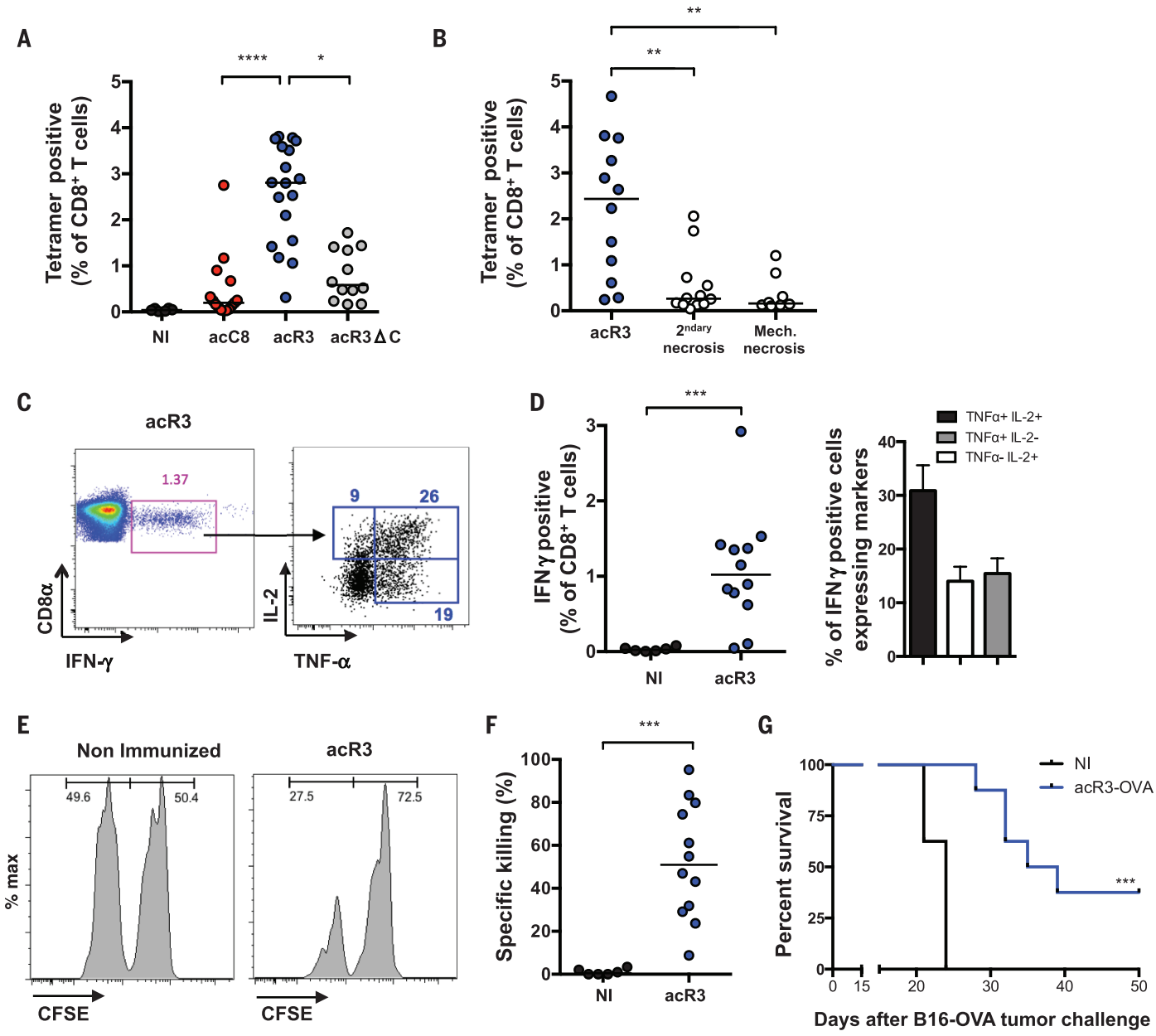

Fig. 2. Necroptotic cells are immunogenic and require RHIM-dependent ripoptosome formation for efficient cross-priming of CD8$^+$ T cells. To elicit cross-priming, we intradermally injected OVA-expressing dying cells (H-2^q) into mice (H-2^b), and we analyzed them on day 9 postimmunization (p.i.). (**A** and **B**) Using K^b-SIINFEKL tetramers, OVA-specific CD8$^+$ T cells were quantified and plotted as a percentage of total CD8$^+$ T cells. Bars indicate medians, and results are pooled from three independent experiments with three to six mice per group (each circle represents one mouse). NI, nonimmunized. (**C** and **D**) We quantified the production of IFN-γ, tumor necrosis factor–α (TNF-α), and IL-2 in response to ex vivo SIINFEKL peptide restimulation. In (C), representative fluorescence-activated cell sorting (FACS) plots are shown, with a pseudo-colored density plot in the left panel. Numbers indicate the percentage of gated cells. In (D), the frequency of IFN-γ–expressing and polyfunctional cells is plotted. Results are pooled from three independent experiments with three to six mice per group and reported as individual mice (each circle represents one mouse). The left panel shows medians as horizontal bars (IFN-γ); the right panel shows means with SEM (error bars) (TNF-α and IL-2). (**E** and **F**) In vivo cytotoxicity assays were performed in acR3-OVA–immunized mice. At day 8 p.i., mice were adoptively transferred with carboxyfluorescein diacetate succinimidyl ester (CFSE)–labeled splenocytes. The frequency of CSFE^{hi} (irrelevant peptide control) and CFSE^{low} (SIINFEKL-loaded) splenocytes (injected at a 1:1 ratio) was determined at day 9. Representative FACS plots are shown in (E), and the percent of specific killing is plotted in (F). In (F), bars indicate medians, and results are pooled from three independent experiments with four mice per group (each circle represents one mouse). (**G**) Tumor challenge experiments were performed, involving the injection of 5 × 10^5 B16F10-OVA cells on day 12 p.i. Results are reported as a survival curve from one representative experiment with 8 to 11 mice per group (n = 2 independent experiments). For (A) and (B), P values were determined by the Kruskal-Wallis test, followed by Dunn's post-test; for (D) and (F), P values were determined by the Mann-Whitney test; and in (G), mice survival percentages were compared using the log-rank test. *P < 0.05; **P < 0.01; ***P < 0.001; ****P < 0.0001.

Downloaded from http://science.sciencemag.org/ on August 30, 2016

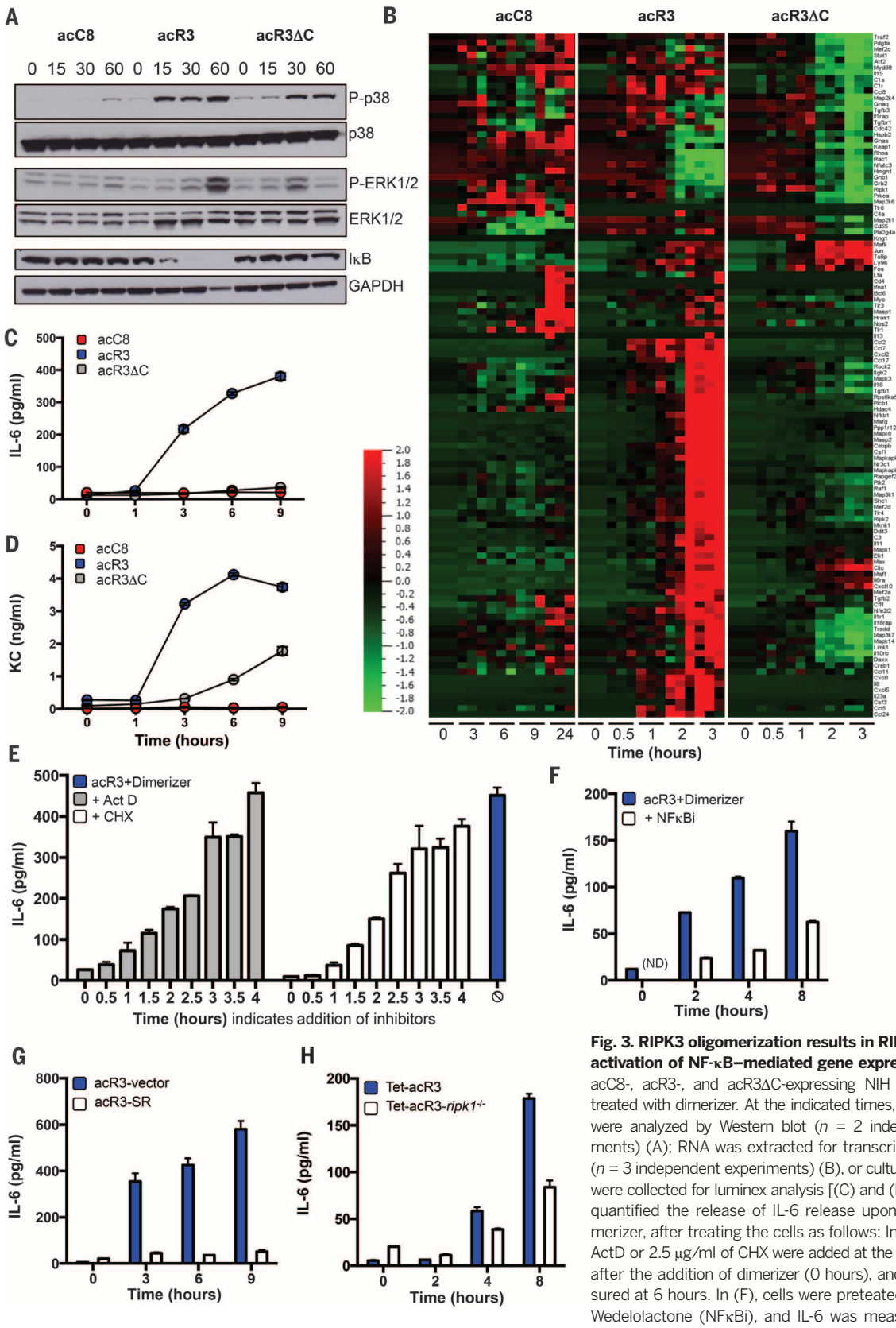

Fig. 3. RIPK3 oligomerization results in RIPK1-dependent activation of NF-κB–mediated gene expression. (**A** to **D**) acC8-, acR3-, and acR3ΔC-expressing NIH 3T3 cells were treated with dimerizer. At the indicated times, protein extracts were analyzed by Western blot (n = 2 independent experiments) (A); RNA was extracted for transcriptional profiling (n = 3 independent experiments) (B), or culture supernatants were collected for luminex analysis [(C) and (D)]. (**E** to **H**) We quantified the release of IL-6 release upon addition of dimerizer, after treating the cells as follows: In (E), 2 μg/ml of ActD or 2.5 μg/ml of CHX were added at the indicated times, after the addition of dimerizer (0 hours), and IL-6 was measured at 6 hours. In (F), cells were preteated with 10 μM of Wedelolactone (NFκBi), and IL-6 was measured at the indicated times. In (G), acR3 cells that were stably expressing the control vector (acR3-vector) or the mutant SR IκB (acR3-SR) were used. In (H), control NIH 3T3 cells (Tet-acR3), and cells lacking RIPK1 and expressing RIPK3 2xFv under a tetracycline promoter (Tet-acR3-*ripk1*$^{-/-}$), were treated overnight with 500 ng/ml of doxycycline before the addition of dimerizer. In (C) to (H), the data are presented as means (± SEM) of triplicates from one representative experiment ($n \geq 2$ independent experiments). The heat map indicates the relative expression of the indicated transcript (red indicates high levels and green indicates low levels of expression).

Downloaded from http://science.sciencemag.org/ on August 30, 2016

and acR3ΔC-expressing NIH 3T3 cells, but they did not efficiently phagocytose live cells (fig. S4, A and B). Moreover, both acR3 and acR3ΔC induced the up-regulation of DC activation markers, whereas acC8-expressing NIH 3T3 cells did not (Fig. 1F and fig. S4C). Similarly, intraperitoneal injection of dimerizer-treated acR3- or acR3ΔC-expressing cells induced higher recruitment of immune cells, as compared with injection of acC8-expressing cells (Fig. 1G). Together, these data suggest that necroptotic cells released DAMPs, induced maturation of DCs in vitro, and induced inflammation in vivo.

To assess the respective immunogenicity of apoptotic and necroptotic cells, we immunized C57BL/6 mice by intradermally injecting 10^6 dimerizer-treated NIH 3T3 cells that stably expressed a nonsecretable form of ovalbumin (OVA) (fig. S5A) (*29*). Cells were exposed to dimerizer immediately before injection, thereby enabling them to undergo cell death in situ. We observed significantly higher $CD8^+$ T cell cross-priming when mice were immunized with cells undergoing RIPK3-mediated necroptosis than with cells undergoing caspase-8–mediated apoptosis (Fig. 2A and fig. S5B; $P < 0.0001$). Immunization with acR3ΔC-OVA NIH 3T3 cells did not result in robust $CD8^+$ T cell cross-priming (Fig. 2A and fig. S5B; $P < 0.01$ in a comparison with acR3-OVA NIH 3T3 cells), indicating that RHIM-dependent interactions are required for the immunogenicity of necroptotic cells.

We next compared the cross-priming efficiency of cells undergoing necroptosis with that of cells undergoing unregulated necrosis, such as "mechanical" necrosis (also called primary necrosis, and achieved by repeated freezing and thawing) or "secondary" necrosis (achieved by incubating apoptotic cells for 24 hours before immunization). We found that mechanical and secondary necrotic cells induced only weak $CD8^+$ T cell responses (Fig. 2B; $P < 0.01$). Although the latter results could be partially explained by the loss of antigen after necrotic membrane permeabilization (fig. S6), the findings suggest that in vivo necroptosis is a more efficient inducer of cross-priming, as compared with apoptotic or necrotic cells.

The efficiency and outcome of antigen cross-presentation have been shown to depend on a subset of $CD8\alpha^+$–$CD103^+$ DCs, whose differentiation is driven by the transcription factor for the *Batf3* gene (*30*). We found that immunization of *Batf3*$^{-/-}$ mice with acR3-OVA cells failed to elicit

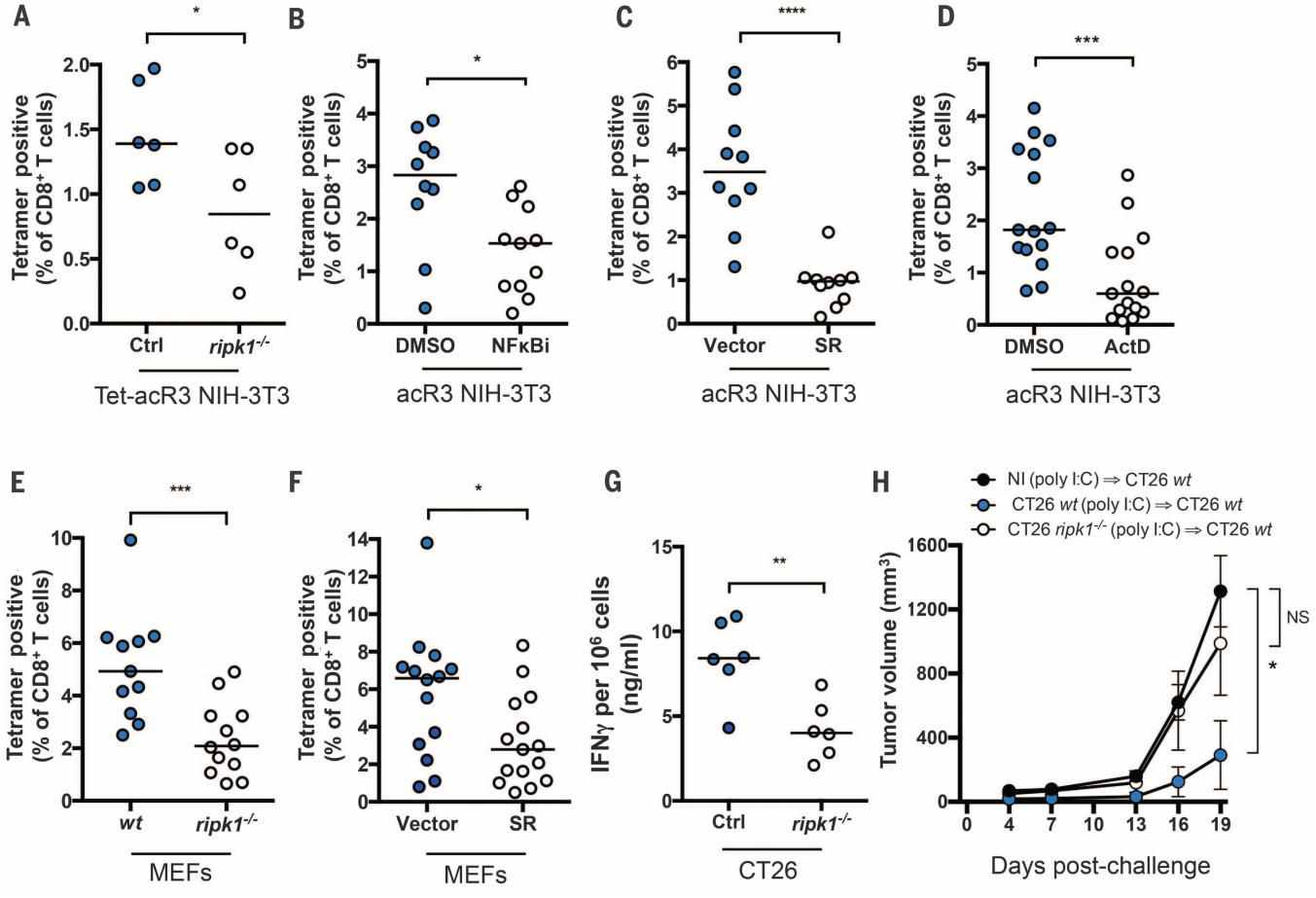

Fig. 4. RIPK1 expression and NF-κB activation during cell death are required for efficient cross-priming and anti-tumor immunity. (**A**) Mice were immunized with Tet-acR3-OVA and Tet-acR3-OVA-*ripk1*$^{-/-}$ NIH 3T3 cells. Data represent one experiment with six mice per group; bars indicate medians. (**B**) acR3-OVA NIH 3T3 cells were pretreated with dimethyl sulfoxide (DMSO) or BAY 11-7085 (NFκBi, 10 μM) for 10 min before the addition of dimerizer and immunization. (**C**) Mice were immunized with acR3-OVA cells expressing NF-κB SR or the control vector. In (**D**), acR3-OVA were pretreated with DMSO or ActD for 45 min before immunization. (**E** and **F**) OVA-expressing MEFs were transfected with 10 μg/ml of poly I:C and, after 6 hours, used for immunization. WT or *ripk1*$^{-/-}$ cells were used in (E); cells expressing the control vector or NF-κB SR were used in (F). Cross-priming was assessed on day 9 p.i. In (B) to (F), results shown are pooled from three independent experiments with three to six mice per group. (**G** and **H**) CT26 control (Ctrl) cells or cells from a CRISPR/cas9 (clustered regularly interspaced short palindromic repeat/CRISPR-associated nuclease 9)–modified line that lacks RIPK1 expression (CT26 *ripk1*$^{-/-}$) were poly I:C–transfected and injected into *Balb/cByJ* mice. Seven days later, spleens and lymph nodes were harvested, and IFN-γ production was quantified (G). In (H), mice were challenged with 5×10^5 WT CT26 cells injected in the opposite flank, and tumor growth was monitored every 3 days. Results are from one representative experiment with six mice per group ($n = 3$ independent experiments). *P* values were determined by the Mann-Whitney test [(A) to (G)] or the two-way ANOVA test (multiple group comparison, comparing each group to the NI group) (H). *$P < 0.05$; **$P < 0.01$; ***$P < 0.001$; ****$P < 0.0001$.

Downloaded from http://science.sciencemag.org/ on August 30, 2016

a $CD8^+$ T cell response (fig. S7, A and B), confirming that cross-presentation of antigen associated with necroptotic cells is mediated by this DC lineage. We next characterized the $CD8^+$ T cells induced by acR3-OVA immunization. $CD8^+$ T cells primed by immunization with necroptotic cells produced multiple effector cytokines (Fig. 2, C and D), exhibited in vivo cytolytic activity (Fig. 2, E and F), and protected mice from tumor challenge (Fig. 2G). Together, these data indicate that necroptotic cells are able to provide both antigen and immune stimulation, in turn supporting DC-mediated cross-priming of $CD8^+$ T cells. The requirement of $RHIM^{RIPK3}$ for the immunogenicity of necroptotic cells suggests that classical DAMPs (e.g., HMGB1) are insufficient to achieve robust cross-priming and supports a critical role for RIPK1, independent of cell death.

To understand the requirement of RHIM for immunogenic necroptosis, we studied the signaling pathways that were engaged during the different forms of cell death and assessed mitogen-activated protein kinase (MAPK) and NF-κB activation after dimerizer treatment. Oligomerization of RIPK3 in acR3-expressing NIH 3T3 cells resulted in the rapid phosphorylation of p38 and extracellular signal–regulated kinase-1 and -2 and the degradation of IκB (Fig. 3A). Activation of these inflammatory pathways was not observed after dimerization of caspase-8 and was attenuated in acR3ΔC-expressing NIH 3T3 cells, with the greatest difference corresponding to the NF-κB pathway (Fig. 3A). To determine the impact on the transcriptional profile, we quantified the mRNA expression of 179 immune-related genes at different stages of cell death (Fig. 3B). Despite the rapid cell death kinetics, full-length RIPK3 activation triggered a significant up-regulation of 72 inflammatory genes, many of which are regulated by NF-κB and MAPK activation (fig. S8A and table S1; rank regression on time with adjustment for false discovery rate, $q < 0.05$). In contrast, we observed only modest changes in dimerizer-treated acC8-expressing cells (three genes differentially expressed) and acR3ΔC-expressing cells (17 genes differentially expressed) (fig. S8A and table S1). We next measured inflammatory cytokines in the supernatant from dimerizer-treated cell cultures and found that acR3 cells released high amounts of IL-6 (Fig. 3C) and CXCL1 (Fig. 3D), validating our transcriptional analysis. IL-6 production was inhibited in a time-dependent manner by treating the cells with actinomycin-D (ActD) or cycloheximide (CHX) (Fig. 3E). These data suggest that necroptotic cells actively transcribe and translate inflammatory cytokines during cell death (fig. S8B). Moreover, chemical inhibition of IKK kinase activity diminished the release of IL-6 (Fig. 3F), and stable expression of an IκB dominant negative protein [NF-κB (S32A, S36A) super repressor, SR] also inhibited cytokine secretion (Fig. 3G).

To formally test the contribution of RIPK1, we deleted RIPK1 from NIH 3T3 cells and stably expressed the RIPK3-2xFv construct under a tetracycline-inducible promoter (Tet-acR3) (fig. S9, A and B). The addition of dimerizer triggered necroptosis in both cell lines (fig. S9C); however, NF-κB activation (fig. S9D) and IL-6 production (Fig. 3H) were reduced in the cells lacking RIPK1. These results revealed an NF-κB transcriptional and translational activity that is engaged during RIPK3 necroptosis.

We next tested the hypothesis that RIPK1 signaling and NF-κB–dependent gene expression within the dying cell are critical for cross-priming. We immunized mice using necroptotic cells that lacked RIPK1 (Tet-acR3-*Ripk1*$^{-/-}$) (Fig. 4A), cells that lacked NF-κB signaling [pretreated with NF-κB inhibitor (NFκBi) (Fig. 4B) or overexpressing the NF-κB SR (Fig. 4C)], or cells in which transcription was inhibited (pretreated with ActD) (Fig. 4D). Cross-priming was significantly reduced in all instances, thus establishing that active RIPK1–NF-κB signaling is essential for the immunogenicity of necroptotic cells.

To extend our findings to a second model that leads to simultaneous RIPK1-dependent NF-κB activation and cell death, we used the transfection of polyinosinic-polycytidylic acid (poly I:C) (fig. S10A), which engages the cytosolic RNA sensors RIG-I and MDA5, in turn recruiting the adaptor proteins IPS-1, RIPK1, TRADD, and FADD (*31*). We confirmed that in this model, RIPK1 was essential for NF-κB activation (fig. S10, B and C) and cytokine secretion (fig. S10D) (*31*). Moreover, poly I:C transfection results in intrinsic apoptosis, rather than necroptosis (*32*). We found that in both wild-type (WT) and *Ripk1*$^{-/-}$ cells, poly I:C is capable of inducing similar levels of caspase-3 activation and cell death (fig. S10, E and F). Thus, we were able to decouple NF-κB activation from apoptosis induction downstream of double-stranded RNA sensors.

We next tested the hypothesis that immunogenic apopotosis induced by poly I:C (*33*) was regulated by the RIPK1–NF-κB axis. We immunized mice with poly I:C–transfected OVA-expressing mouse embryonic fibroblasts (MEFs) (Fig. 4, E and F). Compared with immunization with WT cells, immunization with *Ripk1*$^{-/-}$ (Fig. 4E) or NF-κB SR–expressing cells (Fig. 4F) resulted in a significant reduction in $CD8^+$ T cell priming. These data reinforce the crucial role of RIPK1-mediated NF-κB activation within dying cells during the initiation of $CD8^+$ T cell immune responses, despite the presence of a strong inflammatory pathogen-associated molecular pattern such as poly I:C.

Finally, we tested the relevance of our findings in the context of tumor immunity. Deletion of RIPK1 from poly I:C–transfected CT26 colon carcinoma cells (fig. S10G) rendered them poorly immunogenic in comparison with WT cells, as measured by interferon-γ (IFN-γ) production (Fig. 4G) and protection from tumor challenge (Fig. 4H). Overall, our results reveal RIPK1-induced NF-κB activation as the critical determinant of $CD8^+$ T cell immunity to cell-associated antigens.

The danger model predicts that cell death resulting from tissue damage and stress induces the passive release of preformed danger molecules that mediate subsequent immune responses (*34*). Breaking from this model, the present study reveals an unexpected role for RIPK1- and NF-κB–driven gene expression during cell death as a key determinant for cross-priming of $CD8^+$ T cells. Thus, although the release of DAMPs can trigger inflammatory responses, we show that RIPK1-mediated induction of NF-κB and its downstream target genes is necessary for initiating $CD8^+$ T cell adaptive immunity. To date, PCD pathways have been defined by morphological and biochemical methods; our results highlight the need for a transcriptional definition of cell death, as a means of understanding the relationship between dying cells and immunity. Whether these findings apply to other aspects of adaptive immunity (e.g., B cell or CD4 T cell priming) remains to be determined (*7*, *35*).

NF-κB is a critical regulator of innate immune responses, and its pathway is a prime target of interference by pathogens; our results suggest an additional benefit for microbes that interfere with both NF-κB signaling (*36*) and cell death pathways (*37*, *38*). For example, viral inhibitors of RHIM-dependent interactions (e.g., mouse cytomegalovirus M45) may have evolved to subvert $CD8^+$ T cell cross-priming. In turn, scaffold proteins such as RIPK1, which are an assemblage of multiple domains (RHIM domain, death domain, and kinase domain), may have evolved to coordinate cell death and innate signaling modules (*39*), together orchestrating adaptive immunity. Thus, investigation and targeting of scaffold proteins at the intersection of cell death pathways and host-defense pathways may provide new therapeutic opportunities in the field of immunotherapy.

REFERENCES AND NOTES

1. M. L. Albert, B. Sauter, N. Bhardwaj, *Nature* **392**, 86–89 (1998).
2. M. L. Albert *et al.*, *Nat. Med.* **4**, 1321–1324 (1998).
3. M. J. Bevan, *J. Exp. Med.* **143**, 1283–1288 (1976).
4. S. Turley, L. Poirot, M. Hattori, C. Benoist, D. Mathis, *J. Exp. Med.* **198**, 1527–1537 (2003).
5. S. S. Iyer *et al.*, *Proc. Natl. Acad. Sci. U.S.A.* **106**, 20388–20393 (2009).
6. Y. Shi, J. E. Evans, K. L. Rock, *Nature* **425**, 516–521 (2003).
7. H. Kazama *et al.*, *Immunity* **29**, 21–32 (2008).
8. P. Scaffidi, T. Misteli, M. E. Bianchi, *Nature* **418**, 191–195 (2002).
9. B. Sauter *et al.*, *J. Exp. Med.* **191**, 423–434 (2000).
10. S. R. Scheffer *et al.*, *Int. J. Cancer* **103**, 205–211 (2003).
11. A. F. Ochsenbein *et al.*, *Proc. Natl. Acad. Sci. U.S.A.* **96**, 2233–2238 (1999).
12. J. Gamrekelashvili *et al.*, *J. Clin. Invest.* **123**, 4755–4768 (2013).
13. M. L. Albert, *Nat. Rev. Immunol.* **4**, 223–231 (2004).
14. N. Casares *et al.*, *J. Exp. Med.* **202**, 1691–1701 (2005).
15. M. Obeid *et al.*, *Nat. Med.* **13**, 54–61 (2007).
16. M. Feoktistova *et al.*, *Mol. Cell* **43**, 449–463 (2011).
17. T. Tenev *et al.*, *Mol. Cell* **43**, 432–448 (2011).
18. J. M. Blander, *Nat. Rev. Immunol.* **14**, 601–618 (2014).
19. S. J. Martin, C. M. Henry, S. P. Cullen, *Mol. Cell* **46**, 387–397 (2012).
20. A. Oberst *et al.*, *J. Biol. Chem.* **285**, 16632–16642 (2010).
21. S. Orozco *et al.*, *Cell Death Differ.* **21**, 1511–1521 (2014).
22. S. W. G. Tait *et al.*, *Cell Reports* **5**, 878–885 (2013).
23. C. P. Dillon *et al.*, *Cell* **157**, 1189–1202 (2014).
24. F. Ghiringhelli *et al.*, *Nat. Med.* **15**, 1170–1178 (2009).
25. A. Tesniere *et al.*, *Oncogene* **29**, 482–491 (2010).
26. M. Michaud *et al.*, *Science* **334**, 1573–1577 (2011).
27. O. Schulz, C. Reis e Sousa, *Immunology* **107**, 183–189 (2002).
28. C. Kurts, B. W. S. Robinson, P. A. Knolle, *Nat. Rev. Immunol.* **10**, 403–414 (2010).

Downloaded from http://science.sciencemag.org/ on August 30, 2016

29. D. Sancho *et al.*, *Nature* **458**, 899–903 (2009).
30. K. Hildner *et al.*, *Science* **322**, 1097–1100 (2008).
31. M.-C. Michallet *et al.*, *Immunity* **28**, 651–661 (2008).
32. R. Besch *et al.*, *J. Clin. Invest.* **119**, 2399–2411 (2009).
33. O. Schulz *et al.*, *Nature* **433**, 887–892 (2005).
34. P. Matzinger, *Annu. Rev. Immunol.* **12**, 991–1045 (1994).
35. S. Gallucci, M. Lolkema, P. Matzinger, *Nat. Med.* **5**, 1249–1255 (1999).
36. M. M. Rahman, G. McFadden, *Nat. Rev. Microbiol.* **9**, 291–306 (2011).
37. M. Lamkanfi, V. M. Dixit, *Cell Host Microbe* **8**, 44–54 (2010).
38. N. Yatim, M. L. Albert, *Immunity* **35**, 478–490 (2011).
39. R. Weinlich, D. R. Green, *Mol. Cell* **56**, 469–480 (2014).

ACKNOWLEDGMENTS

The authors thank S. Zelenay for the LA-ΔOVA-mCherry and ΔOVA-mCherry constructs; R. Weil for the dominant negative NF-κB plasmid; P.O. Vidalain for the NF-κB–Luciferase reporter plasmid; P. Fitzgerald for cell lines; and M.A. Ingersoll, D. Duffy, O. Schwartz, J. Boussier, and A. Yatim for their critical reading of the manuscript and advice. We also thank M. A. Ingersoll for mouse protocols, M. Fontes for assistance with Qlucore Omics software, and the Centre for Human Immunology for providing technical support and project management. The data from this study are tabulated here and in the supplementary materials. Dimerizable RIPK3 and caspase-8 constructs are available from D.O. under a materials transfer agreement with the University of Washington. U.S. Patent PCT/US2014/036196 has been filed by St. Jude Children's Research Hospital, covering the induction of necroptosis using RIPK3 oligomerization. Funding for the work was provided by the Agence Nationale de Recherches sur le Sida et les Hepatitis; Projet ANUBIS of the Agence Nationale de la Recherche (ANR-12-BSV3-0011-01) and a Laboratories of Excellence Immuno-Onco grant (ANR-11-IDEX-0005-02) (M.L.A., N.Y., H.J.-S., and R.B.d.S.); the French National Cancer Institute (INCa) (Plan Cancer 2014–2019) and the Ecole de l'Inserm Liliane Bettencourt (N.Y.); NIH grants R21CA185681 and R01AI108685 (A.O.); NIH grant AI44848 (D.R.G.); and NIH award 5R01AI108685-02 (S.O.). C.R.S. and O.S. were supported by grants from Cancer Research UK, The Francis Crick Institute, and the European Research Council. The authors thank the Genomics Platform of the Department of Translational Research at Institut Curie for experiments conducted using Nanostring tools (grants INCa-DGOS-4654, SIRIC11-002, ANR-10-IDEX-0001-02 PSL, and ANR-11-LBX-0044).

SUPPLEMENTARY MATERIALS

www.sciencemag.org/content/350/6258/328/suppl/DC1
Materials and Methods
Figs. S1 to S11
Table S1
References (*40*–*48*)
Movies S1 to S3

16 July 2015; accepted 11 September 2015
Published online 24 September 2015
10.1126/science.aad0395

T CELL IMMUNITY

Stable inhibitory activity of regulatory T cells requires the transcription factor Helios

Hye-Jung Kim,[1,2] R. Anthony Barnitz,[3,4] Taras Kreslavsky,[1,2] Flavian D. Brown,[3] Howell Moffett,[1] Madeleine E. Lemieux,[5] Yasemin Kaygusuz,[1] Torsten Meissner,[1,2] Tobias A. W. Holderried,[1,2] Susan Chan,[6,7] Philippe Kastner,[6,7] W. Nicholas Haining,[3,4,8] Harvey Cantor[1,2]*

The maintenance of immune homeostasis requires regulatory T cells (T_{regs}). Given their intrinsic self-reactivity, T_{regs} must stably maintain a suppressive phenotype to avoid autoimmunity. We report that impaired expression of the transcription factor (TF) Helios by FoxP3$^+$ CD4 and Qa-1–restricted CD8 T_{regs} results in defective regulatory activity and autoimmunity in mice. Helios-deficient T_{regs} develop an unstable phenotype during inflammatory responses characterized by reduced FoxP3 expression and increased effector cytokine expression secondary to diminished activation of the STAT5 pathway. CD8 T_{regs} also require Helios-dependent STAT5 activation for survival and to prevent terminal T cell differentiation. The definition of Helios as a key transcription factor that stabilizes T_{regs} in the face of inflammatory responses provides a genetic explanation for a core property of T_{regs}.

Regulatory T cells (CD4 and CD8 T_{regs}) dampen excessive immune responses and prevent or ameliorate autoimmune tissue damage, whereas immune suppression exerted by T_{regs} can impede anti-tumor immune responses. In contrast to effector T cells (T_{eff}), which rely on robust activation and differentiative plasticity, T_{regs} depend on the preservation of a stable, anergic, and suppressive phenotype to maintain immune homeostasis (*1*, *2*). Although FoxP3$^+$ CD4 T_{regs} are remarkably stable (*1*, *2*), the genetic mechanisms that ensure phenotypic stability after expansion during inflammation, infection, or autoimmunity (i.e., conditions that most require maintenance of an anergic and inhibitory T_{regs} phenotype) are poorly understood.

The Helios (Ikzf2) transcription factor (TF) is expressed by two T_{reg} lineages: FoxP3$^+$CD4$^+$ and Ly49$^+$CD8$^+$ T_{regs} (fig. S1) (*3*–*6*). To determine the contribution of Helios to the regulatory phenotype, we analyzed mice deficient in *Ikzf2* (*Helios*$^{-/-}$), the gene that encodes Helios (*5*). *Helios*$^{-/-}$ mice (6 to 8 weeks old) displayed reduced numbers of CD8 but not CD4 T_{regs} (fig. S2) and no obvious signs of autoimmune disorder. However, 5-month-old Helios-deficient mice exhibited increased numbers of activated CD4 and CD8 T cells, T follicular helper (T_{FH}) cells, and germinal center (GC) B cells as compared to wild-type (WT) mice (Fig. 1A and fig. S3A). Autoimmune disease was apparent by 6 to 8 months of age, accompanied by the infiltration of immune cells into nonlymphoid tissues (Fig. 1B), the production of autoantibodies (Fig. 1C), and glomerular nephritis (fig. S3B). *Rag2*$^{-/-}$ mice reconstituted with bone marrow (BM) from *Helios*$^{-/-}$ donors also developed autoimmunity (fig. S4), indicating a lymphocyte-intrinsic effect.

Although *Helios*$^{-/-}$ mice did not develop overt signs of autoimmunity until 5 to 6 months of age, upon challenge with viral infection by LCMV-Armstrong (LCMV, lymphocytic choriomeningitis virus), both young (2 months) and older (6 months) *Helios*$^{-/-}$ mice but not *Helios*$^{+/+}$ mice developed inflammatory and autoimmune changes characterized by increased levels of T_{FH} and GC B cells (Fig. 1D) and immunoglobulin G (IgG) deposition in the kidney (Fig. 1E), although *Helios*$^{+/+}$ and *Helios*$^{-/-}$ mice cleared virus with equal efficiency (fig. S5).

Because autoimmunity in *Helios*$^{-/-}$ mice did not result from defective negative selection (figs. S6 to S8), we asked whether it instead reflected defective T_{reg} activity. Analyses of BM chimeras that express a selective Helios deficiency in either CD4 or CD8 T cells revealed that mice with either Helios-deficient CD4 or CD8 T cells develop autoimmune disease with similar features (fig. S9). Moreover, tolerance was dominant, because *Rag2*$^{-/-}$ mice given Helios$^{-/-}$ BM + Helios$^{+/+}$ BM did not develop autoimmunity (fig. S10).

Direct evidence for the contribution of Helios to CD4 T_{reg} activity and the prevention of autoimmune disease came from analysis of Helios$^{fl/fl}$.FoxP3^{YFP}-Cre mice, which develop autoimmune disease at >5 months of age, characterized by increased numbers of activated CD4 and CD8 T cells, T_{FH} and GC B cells (Fig. 2, A and B), autoantibody production (Fig. 2C), and immune cell infiltration (fig. S11). Moreover, BM chimeras from Helios$^{fl/fl}$.FoxP3-Cre donors developed this disorder within 6 weeks (fig. S12).

Helios-sufficient but not Helios-deficient FoxP3$^+$ CD4 T_{regs} exerted dominant, lymphocyte-intrinsic inhibition that prevented autoimmune disease in the presence of highly activated self-reactive T cells from scurfy mice, which have no FoxP3 forkhead domain. BM chimeras reconstituted with Helios$^{-/-}$/Scurfy BM but not Helios$^{+/+}$/Scurfy BM

[1]Department of Cancer Immunology and Virology, Dana-Farber Cancer Institute, 450 Brookline Avenue, Boston, MA 02215, USA. [2]Department of Microbiology and Immunobiology, Division of Immunology, Harvard Medical School, Boston MA. [3]Department of Pediatric Oncology, Dana-Farber Cancer Institute, 450 Brookline Avenue, Boston, MA 02215, USA. [4]Department of Pediatrics, Boston Children's Hospital, Boston, MA, USA. [5]Bioinfo, Plantagenet, Canada. [6]Institut de Génétique et de Biologie Moléculaire et Cellulaire (IGBMC), INSERM U964, CNRS UMR 7104, Université de Strasbourg, 67404 Illkirch, France. [7]Faculté de Médecine, Université de Strasbourg, Strasbourg, France. [8]Broad Institute of MIT and Harvard, Cambridge, MA, USA.
***Corresponding author. E-mail: harvey_cantor@dfci.harvard.edu**

Downloaded from http://science.sciencemag.org/ on August 30, 2016

RIPK1 and NF-κB signaling in dying cells determines cross-priming of CD8 $^{+}$ T cells
Nader Yatim, Hélène Jusforgues-Saklani, Susana Orozco, Oliver Schulz, Rosa Barreira da Silva, Caetano Reis e Sousa, Douglas R. Green, Andrew Oberst and Matthew L. Albert (September 24, 2015)

Science **350** (6258), 328-334. [doi: 10.1126/science.aad0395] originally published online September 24, 2015

Editor's Summary

Dying to impress the immune system

Besides reacting to microbes, T cells can also mount immune responses to fragments of dying cells, which they encounter displayed on dendritic cells. Not all dying cells activate T cells, however, so what differentiates the dying cells that do? Yatim *et al.* studied two forms of programmed cells death: apoptosis and necroptosis. Using mouse cells in culture and mouse models of inflammatory cell death and anti-tumor immunity, they found that programmed cell death initiated T cell immunity only when the dying cells signaled through the enzyme RIPK1 and the transcription factor NF- κB.

Science, this issue p. 328

This copy is for your personal, non-commercial use only.

Article Tools Visit the online version of this article to access the personalization and article tools:
http://science.sciencemag.org/content/350/6258/328

Permissions Obtain information about reproducing this article:
http://www.sciencemag.org/about/permissions.dtl

Science (print ISSN 0036-8075; online ISSN 1095-9203) is published weekly, except the last week in December, by the American Association for the Advancement of Science, 1200 New York Avenue NW, Washington, DC 20005. Copyright 2016 by the American Association for the Advancement of Science; all rights reserved. The title *Science* is a registered trademark of AAAS.

Downloaded from http://science.sciencemag.org/ on August 30, 2016